A CFD PROCESS CHAIN FOR SIMULATING OPEN WINDTUNNEL TEST SECTIONS

V. Ciobaca[1], S. Melber-Wilkending[2] and M. Pott-Pollenske[3]

Deutsches Zentrum für Luft und Raumfahrt, DLR, Braunschweig, Germany, 38108

This paper discusses a CFD procedure for simulating open wind tunnel test sections based on the investigations of the DLR project ForMEx II. Within this project numerical simulations and the analysis of the wind tunnel (w/t) experiments are performed in order to study the potential of CFD to support and improve the w/t corrections. In this paper, the aerodynamic low speed w/t DNW-NWB and the aeroacoustic w/t AWB are investigated. First, computations for the empty test sections are conducted, for the evaluation of the CFD potential to simulate the open jet flow in each of the w/ts, and second, the open jet flow with the DLR F16 2D high-lift model installed, for the aeroacoustic AWB w/t. The overall good agreement of the numerical results compared to the experiments indicate a reliable capability to simulate and further support the development and adjustment of the tunnel corrections for open test sections.

1 Introduction and outline

For the design of novel configurations the w/t experiment is still an indispensable tool in order to predict the aerodynamic and the aeroacoustic performance, and to validate the numerical procedure. Still, certain inaccuracies are present in the data corrections of the w/t experiments performed for minimizing the influence of the w/t boundaries and mounting effects. The tunnel boundaries are represented by solid walls for the closed section, respective free shear layers for the open test section. During the last years with the help of advanced modern procedures for CFD flow simulations numerous investigations have been conducted for tunnel test sections. In this sense, for closed test sections, an example is the work performed within the DLR project ForMEx, [1, 2], where numerical simulations and accordingly the analysis of the tunnel experiments were performed in order to improve the wind tunnel testing technique. The closed sections of the low speed facility DNW-NWB and the transonic wind tunnel ETW with specific aircraft models have been investigated in detail. On the one hand, the closed tunnel sections are preferred for aerodynamic measurements, while on the other hand, the open test sections are of great importance for acoustic experiments. The CFD simulations may serve as a tool in order to examine also the flow in open test sections with the required accuracy and justified effort.

Within the DLR ForMEx II project, one of the objectives is to investigate the potential of CFD to support the w/t testing in open tunnel sections. Here, we focus on the low speed facilities, DNW-NWB and AWB. The studies are intended towards identifying the limits of the existing wind tunnel correction methods and the possibility to lead to certain improvements. This work will serve also for the validation and the potential improvement of numerical methods, so that in the near future the w/t boundaries and mounting effects may be analyzed for a specific model in advance of or after a measurement campaign, or even taken into account during the model design phase.

Based on the ForMEx II project work, this paper shows the CFD potential to simulate open tunnel sections with a good accuracy. The verification of the numerical results with tunnel data for empty test sections and for a 2D high lift configuration in the aeroacoustic w/t AWB are presented here.

2 Wind Tunnels and Model description

2.1 DNW-NWB wind tunnel

The low speed facility DNW-NWB (Figure 1a) is located in Braunschweig, Germany and is an atmospheric closed loop wind tunnel, [3]. The facility may be used with a closed - as well as with an open-test section for a wide range of aerodynamic investigations (Figure 1a). The maximum velocity in the closed test section is 85 m/s, where for the open

[1] Research Scientist, Institute of Aerodynamics and Flow Technology, Transport Aircrafts, vlad.ciobaca@dlr.de

[2] Research Scientist, Institute of Aerodynamics and Flow Technology, Transport Aircrafts, Stefan.Melber@dlr.de

[3] Research Scientist, Institute of Aerodynamics and Flow Technology, Technical Acoustics, Michael.Pott-Pollenske@dlr.de

section a top speed of 70 m/s may be achieved. The study is focused on the open jet wind tunnel configuration, where the nozzle end has a rectangular shape of 3.25 m in width and 2.8 m in height, and the air collecting system is represented by an aerodynamically optimized Prandtl ring with breather gaps (Figure 1b). The maximum Reynolds-number based on $0.1*\sqrt{S}$ is $1.7*10^6$, where S is the cross-sectional area of the test section.

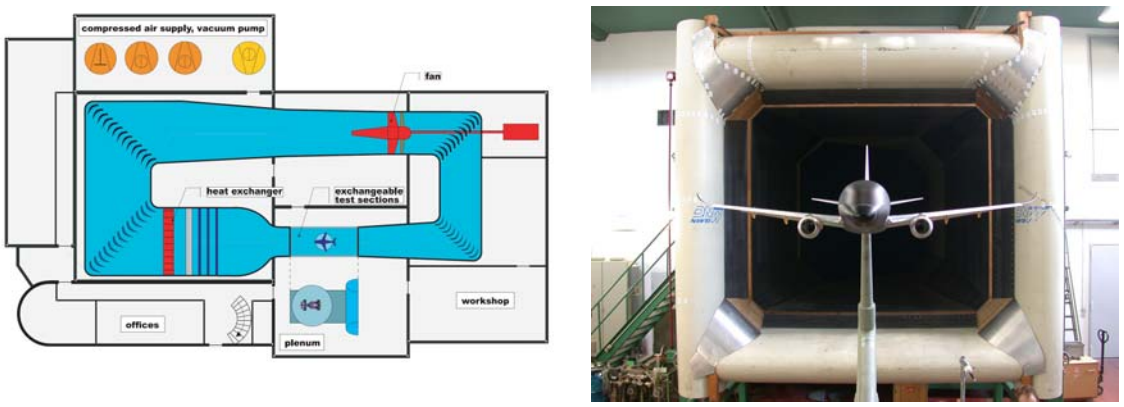

(a) Cross-section of the NWB tunnel (b) Collector of the NWB tunnel

Figure 1 DNW-NWB wind tunnel

2.2 AWB wind tunnel

The aeroacoustic facility AWB (Akustischer Windkanal Braunschweig) is also an atmospheric closed loop w/t (Figure 2a). Due to acoustic purposes it is limited to measurements in an open test section for various configurations, e.g. from single element airfoils to high-lift models. The end section of the nozzle has a rectangular shape of 0.8 m in width and 1.2 m in height. In general, the 2D models are installed between side plates with turntables, designed in prolongation of the nozzle (Figure 2b). In contrast to the NWB set-up, the AWB collector is aeroacoustically optimized providing a very large cross-section that enables the intake of both the core flow and the free shear layer. An interesting feature of the collector is the ability to be translated in X and Z axis, allowing to capture the flow also for measurements at high angles of attack. The maximum tunnel speed is 65 m/s and the maximum Reynolds-number based on $0.1*\sqrt{S}$ is $0.4*10^6$, where S is the cross-sectional area of the nozzle exit section.

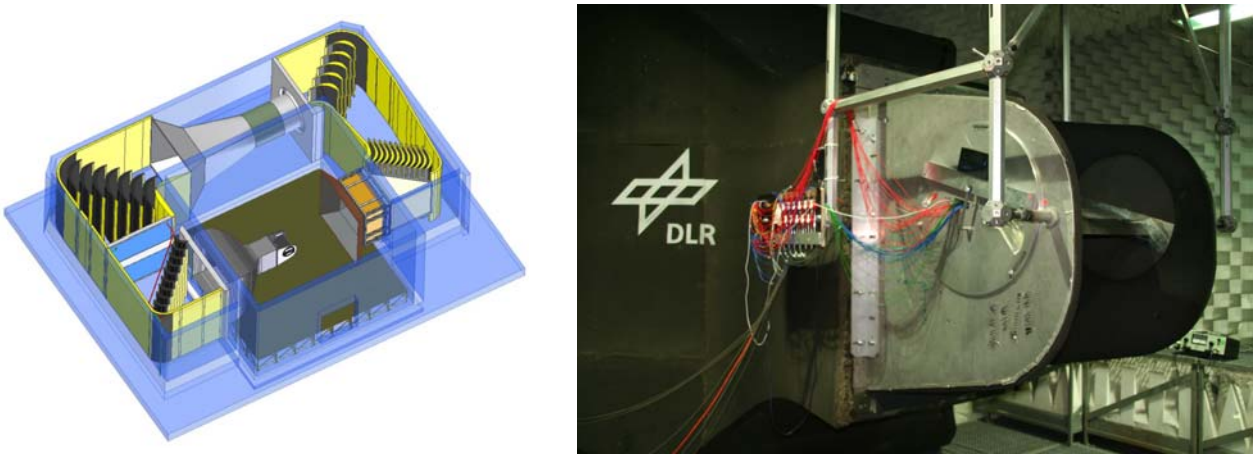

(a) Overview of the tunnel (b) Mounting system for 2D models in AWB tunnel

Figure 2 AWB wind tunnel

2.3 DLR F16 High Lift model

The DLR F16 model is a multi element 2D high lift airfoil. The modular design of the F16 allows to perform tests in a 2 elements configuration, e.g. clean or droop nose, as well as in a 3 elements configuration with slat and flap. In the present paper, only the 3 elements configuration will be discussed,[4]. Figure 3 shows a sketch of the high lift airfoil. The model chord length is c=300 mm, and in span wise direction, from side plate to side plate it measures 800mm. The

high lift devices, flap and slat, are deflected with 30 degrees each ($\delta_F = \delta_S = 30^o$) with the corresponding gap and overlap values normalized with the model chord: g_F= 1%, ovl_F=1% and g_S= 2.3%, ovl_S=-1%. The model is being used extensively in several common research projects at DLR as well as in European framework projects, like e.g. TIMPAN.

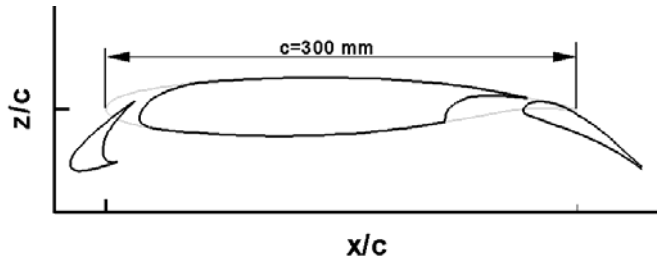

Figure 3 F16 High Lift Airfoil

3 Numerical approach to simulate open tunnel test sections

3.1 Numerical method

The solution of the Reynolds-Averaged Navier-Stokes equations is carried out using the hybrid unstructured DLR-TAU code [5], where for the turbulence modeling the two-equation Menter SST k-ω model is applied, [6]. Due to low Mach number and the resulting stiffness of the RANS equations, low Mach number preconditioning is used. To increase the convergence, an implicit time-integration (LU-SGS) is implemented in the TAU code. All shown results are computed with fully turbulent flow.

All geometrical and aerodynamic conditions are considered. The computational domain includes the nozzle, the air collecting system and the corresponding measurement chamber.

3.2 Tunnel flow speed calibration

The numerical flow speed control in the computed w/t is achieved similar to the measurement systems used in the real wind tunnel. For these open test sections with experimental models inside, the speed control is performed by using the static pressure measurement on the side walls of the nozzle (the average value for several locations) together with a calibration curve of the empty tunnel. In Figure 4 the numerical procedure is exemplified for an open test section. The calibration is performed using measurements with one total pressure probe at the nozzle inlet (p_{tv}), and two static pressure probes on the sidewalls (p_{s1D} and p_{s3D}), together with total and static pressure data in the jet core, at future model location (p_{t_sonde} and p_{s_sonde}). In this way the dependency of the dynamic pressure, representing the tunnel speed, and the difference pressure DPD may be plotted as q=f(DPD). The resulting coefficients of the 2nd order polynomial function are later used for computations with various w/t models.

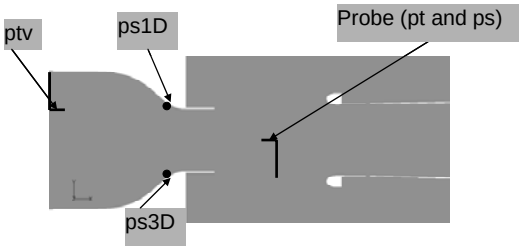

$$p_{s13D} = \frac{p_{s1D} + p_{s3D}}{2}$$

$$DPD = p_{tv} - p_{s13D}$$

$$q = p_t - p_s$$

$$q = a_0 + a_1 \cdot DPD + a_2 \cdot DPD^2$$

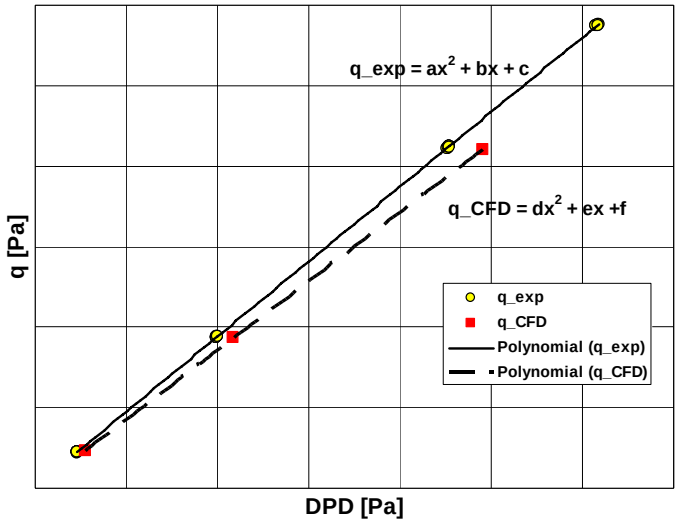

Figure 4 Numerical windtunnel flow speed control

4 CFD validation and verification of the empty tunnel flows

In order to validate the numerical results against the experiments the following guidelines have been used. The validation started with the assessment of the boundary layer in the nozzle, followed by the determination of velocity profiles downstream the nozzle at numerous locations and finally the analysis of the pressure distribution along the tunnel axis. Attention has been paid also to the flow topology of the air collecting system, or e.g. in case of the DNW-NWB to the flow through the breather gaps. Here, for the empty tunnel flow assessment, the grid refinement impact will be exemplified for the AWB tunnel, with velocity profiles downstream of the nozzle. For the sake of brevity, the comparison of boundary layer data as well as pressure distribution along the tunnel axis will be shown only for the NWB tunnel.

4.1 AWB

An extensive w/t measurement campaign was conducted in order to provide sufficient data for comparison with CFD results. By means of a 7-hole-probe the velocity field was measured downstream of the nozzle for several locations, at X = {33, 400, 800, 1200, 1600, 2000} mm, where the X=0 position corresponds to the nozzle exit plane. The velocity components U, V and W were provided for the empty tunnel configuration without end plates and with the collector set to the default position.

For the same tunnel configuration numerical simulations were conducted and compared to experimental data. Here, an initial emphasis was laid on the mesh refinement impact on the flow topology. The first unstructured mesh, shown in Figure 5, had 9.4 million nodes, where for resolving the boundary layer (BL), e.g. in the nozzle, 34 prisms stacks were generated. As an overview, the mean velocity for Y=0, tunnel middle plane, is plotted in Figure 6. The comparison to experimental data revealed that the jet velocity profiles close to the nozzle exit are quite weak in relation to the real flow, while further downstream, matched well (Figure 7, coarse grid, black lines). In this sense, the mesh refinement was focused on the nozzle region, respective downstream the nozzle for a better discretization of the shear layer. Two progressively refined meshes were further used for computing the empty tunnel. The jet velocity profiles are plotted with respect to the grid refinement in Figure 7. The medium (MG, 16 mil. nodes) and fine (FG, 26 mil. nodes) meshes show almost no difference in the results, and match well the experiments. Both, the jet core and the gradient of the mean flow velocity are in good agreement with the measurements, which was not always the case for the coarse grid (CG). In order to tentatively quantify the mesh refinement study, the relative deviations for the integral of velocity profiles are shown in Figure 8. The variable ΔInt is defined as:

$$\Delta Int = \frac{\int_{z_0}^{z_1} \frac{U^{\exp}}{U_0^{\exp}} dz - \int_{z_0}^{z_1} \frac{U^{CFD}}{U_0^{CFD}} dz}{\int_{z_0}^{z_1} \frac{U^{\exp}}{U_0^{\exp}} dz}$$

Large deviations are observed for the initial coarse mesh, while for the other two only differences below 0.5 % are computed. The well resolved velocity profiles indicated that the approach used for the generation of the middle mesh (MG) is sufficient and will be further used for computations including w/t models in the AWB.

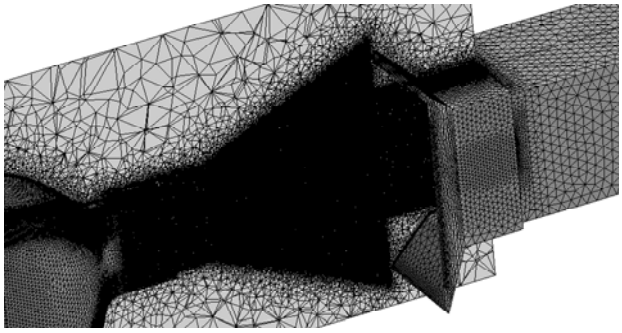

Figure 5 AWB tunnel, mesh overview

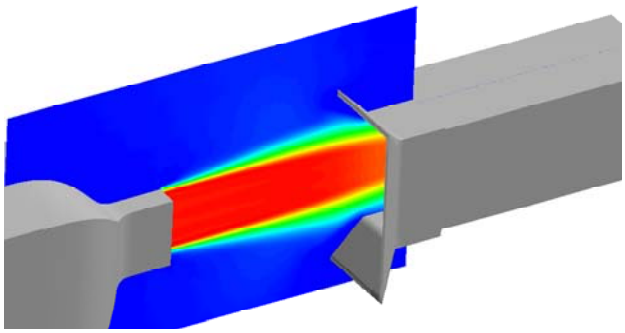

Figure 6 Mean velocity for Y=0 plane in AWB w/t

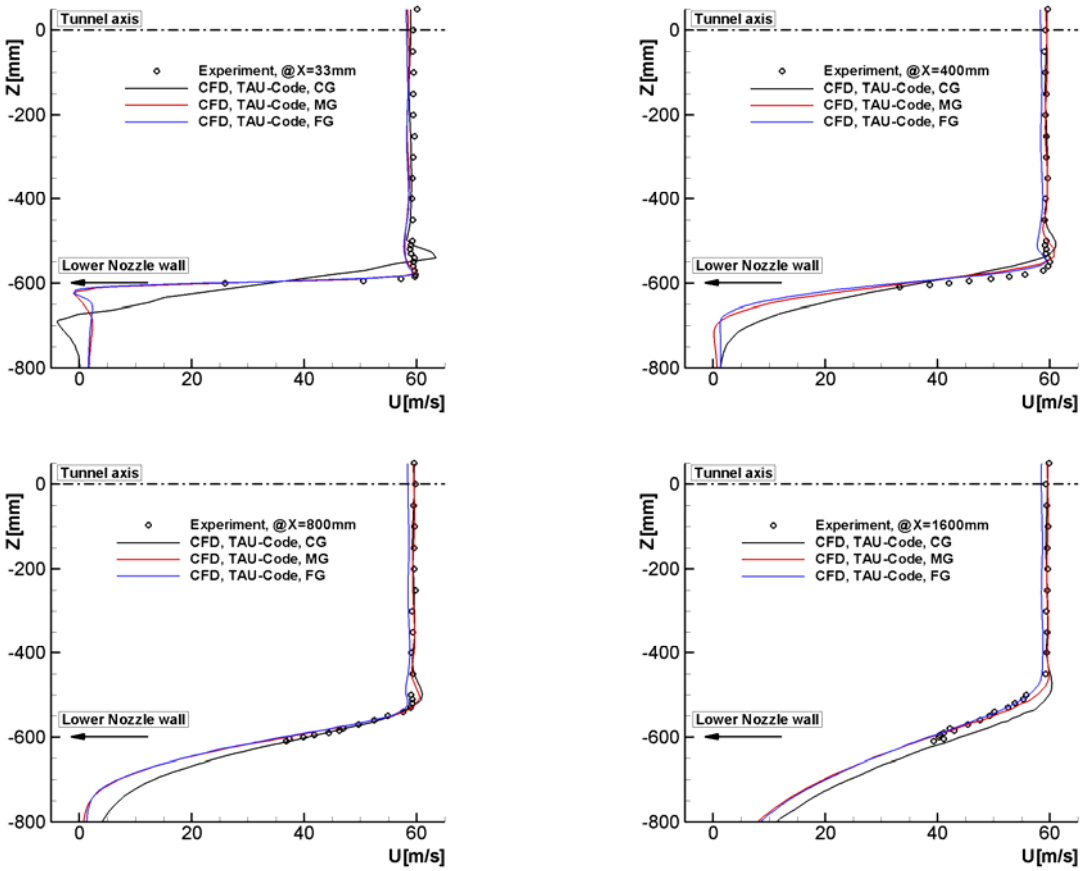

Figure 7 Jet velocity profiles, at Y=0

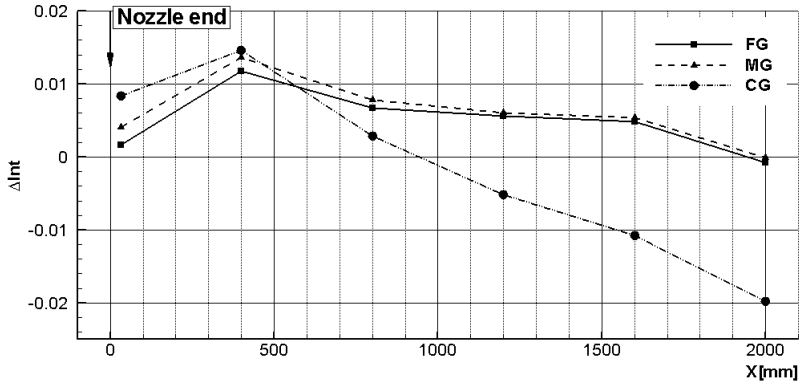

Figure 8 Relative deviations of the velocity profiles in the open jet based on the mesh refinement study

4.2 DNW-NWB

The simulations for the NWB empty tunnel have been carried out for comparison with experimental data and verification of the numerical approach considering now a larger cross-section and an aerodynamical setup of the air collecting system compared to AWB tunnel. Figure 9 shows an overview of the streamwise velocity for a middle plane in the tunnel. One characteristic of the open test section is the pressure distribution along the tunnel axis (Figure 10). In the early design of the DNW-NWB tunnel it was targeted to reach a constant static pressure distribution for the whole test section region, where the design variables were the collector surfaces and the shape of the vortex generators located at nozzle end, [7]. For low velocities (up to 40 m/s), measurements of the empty test section have been carried out also without the vortex generators (at nozzle end) in order to reduce the geometrical complexity, and to facilitate the comparison with CFD results. In the simulations the geometry of the vortex generators was not taken into account, correspondingly. The numerical results show a very good agreement with the experiments for the entire test section.

Only slight deviations were observed for the collector flow. These differences may result due to the RANS approach, where the experimental observations showed the presence of unsteady flow interactions between the jet shear layer and the collector surface. Concerning the nozzle flow, boundary layer data measured on the lower wall and a side wall close to the nozzle outlet are shown in Figure 11 for 70 m/s flow speed. A good agreement of the computational results was observed in comparison to the experiments for all the locations and flow speeds (not shown here).

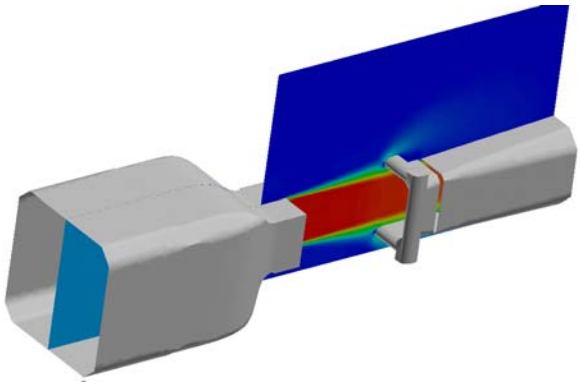

Figure 9 Streamwise velocity contours for a middle test section plane, DNW-NWB w/t

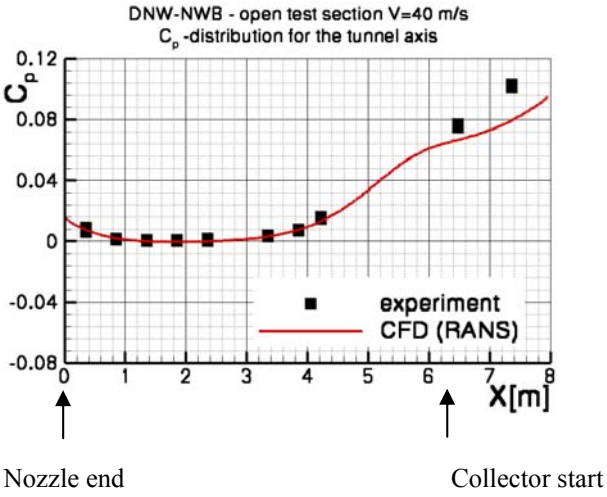

Figure 10 Pressure distribution along the tunnel axis

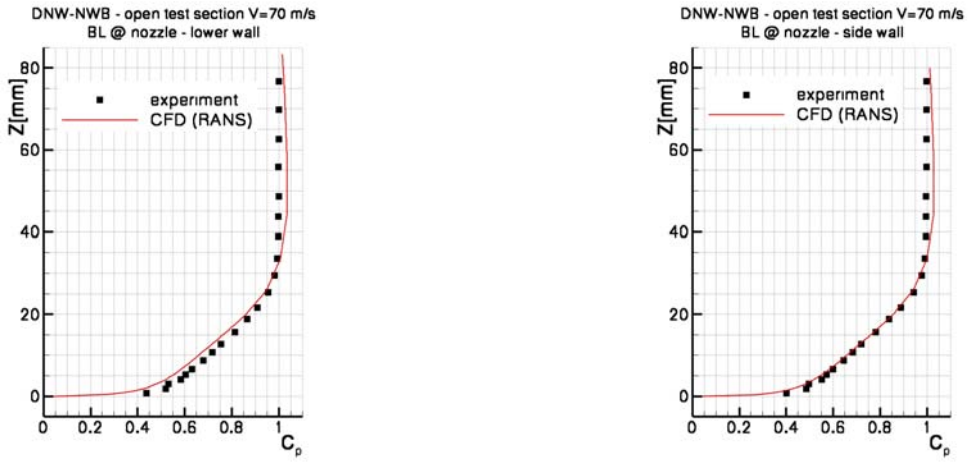

Figure 11 Boundary layer velocity distribution in the nozzle of the DNW-NWB w/t

5 High-Lift Model DLR F16 in AWB tunnel

The tunnel mesh was generated in agreement with the achievements for the empty tunnel results, and was consistent with the medium mesh (MG) discussed in section 4.1. The w/t grid included the geometry of the side plates, while for the mesh surrounding the DLR F16 model the chimera technique was applied. By means of the chimera approach and the motion module from the DLR TAU-Code computations have been performed for a wide range of geometrical angles of attack. For the F16 model, 116 000 nodes were spent on the surface, for the BL discretization 30 points were allocated, and the resulting complete tunnel mesh (including the F16 model) consisted of $22*10^6$ nodes. In Figure 12 the model surface mesh and the middle tunnel plane grid are depicted. Based on this mesh, RANS simulations have been carried out for angles of attack of up to 29 degrees. The collector position was adjusted to a more upstream position Δx=1000mm closer to the nozzle and vertically down (Δz=400mm) compared to the empty tunnel configuration in order to capture the jet deflected by the high-lift model. The mean velocity distributions for the symmetry plane of the tunnel Y=0 are plotted in Figure 13 for 11 and 21 degree, geometrical angle of attack. It is obvious that the deflected jet is well captured by the collector, which would not have been the case for the default setting.

The pressure distribution, taken for the middle section, matches well the experiments, with small deviations for the slat and leading edge region of the main wing (Figure 14). The numerical analyses have been performed fully turbulent, which is in contrast to the experiments, where natural laminar to turbulent transition took place. Still, for the main wing, the computed pressure suction peek is of the same size as in the experiments, only more upstream. Further investigations within the ForMEx II project will study the influence of transition fixing for the DLR F16 model (based on numerical estimations for free field conditions), along with existing experimental data analysis.

The lift polar, Figure 15, resulted as a variation of lift to geometrical angle of attack, so without tunnel corrections, indicates a good agreement of the CFD results with the experiments for the linear region, with a poor approximation of the maximum lift region. On one hand, in the numerical results the lift values are computed for the entire model, on the other hand, the experimental values are calculated based on the pressure distribution measured in one section. The low number of pressure probes has also an influence on the accuracy of lift values in the experiment. In this sense the lift curves should be seen as early results achieved within the ForMEx II project.

Here, not only the capability of RANS modelling to predict the maximum lift is an open issue, but also the tunnel side walls effects play an important role. As indicated in the pressure distributions, the numerical results showed the presence of a separation region on the flap, for the whole range of angles of attack computed. With the increase of angle of attack the length of the separation region was reduced in span direction due to the flow deviations near the side walls (Figure 16). The tendency is definitely consistent with the experiments, only the amount of separation is still under investigation. In Figure 17, the oil flow pictures from the experiments show the presence of a recirculation region on the flap of the F16 model, accompanied by stronger side wall effects with increasing the angle of attack compared to the numerical results.

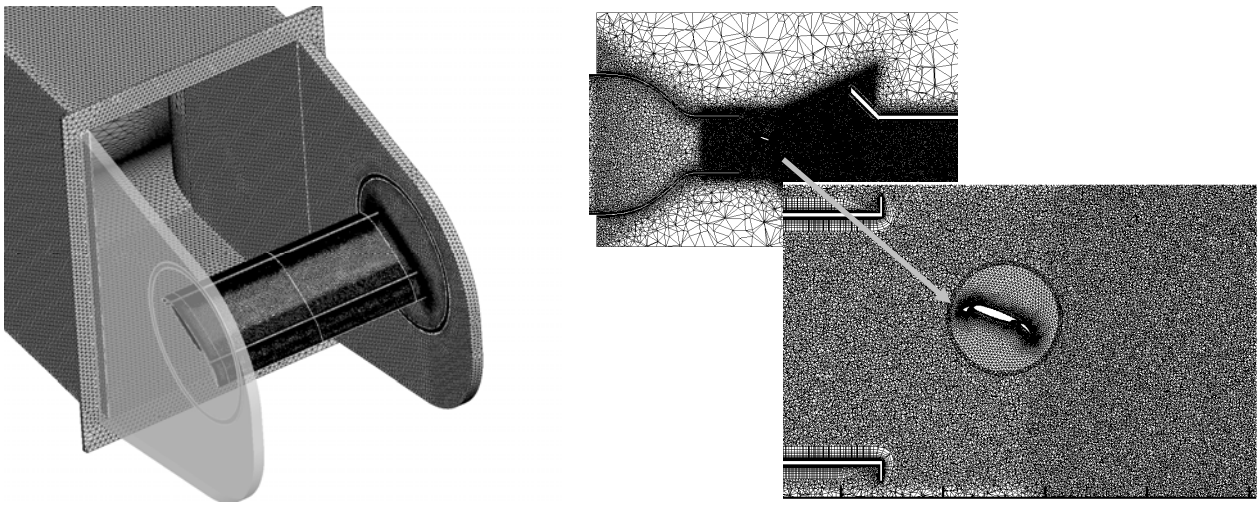

Figure 12 Mesh overview for AWB w/t with DLR F16 model

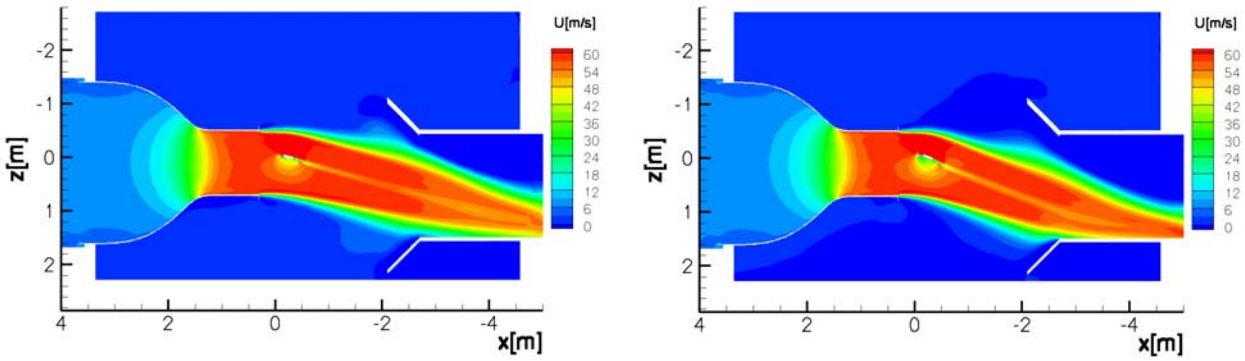

(a) α=11^o (b) α=21^o

Figure 13 Mean velocity in AWB w/t with F16 model

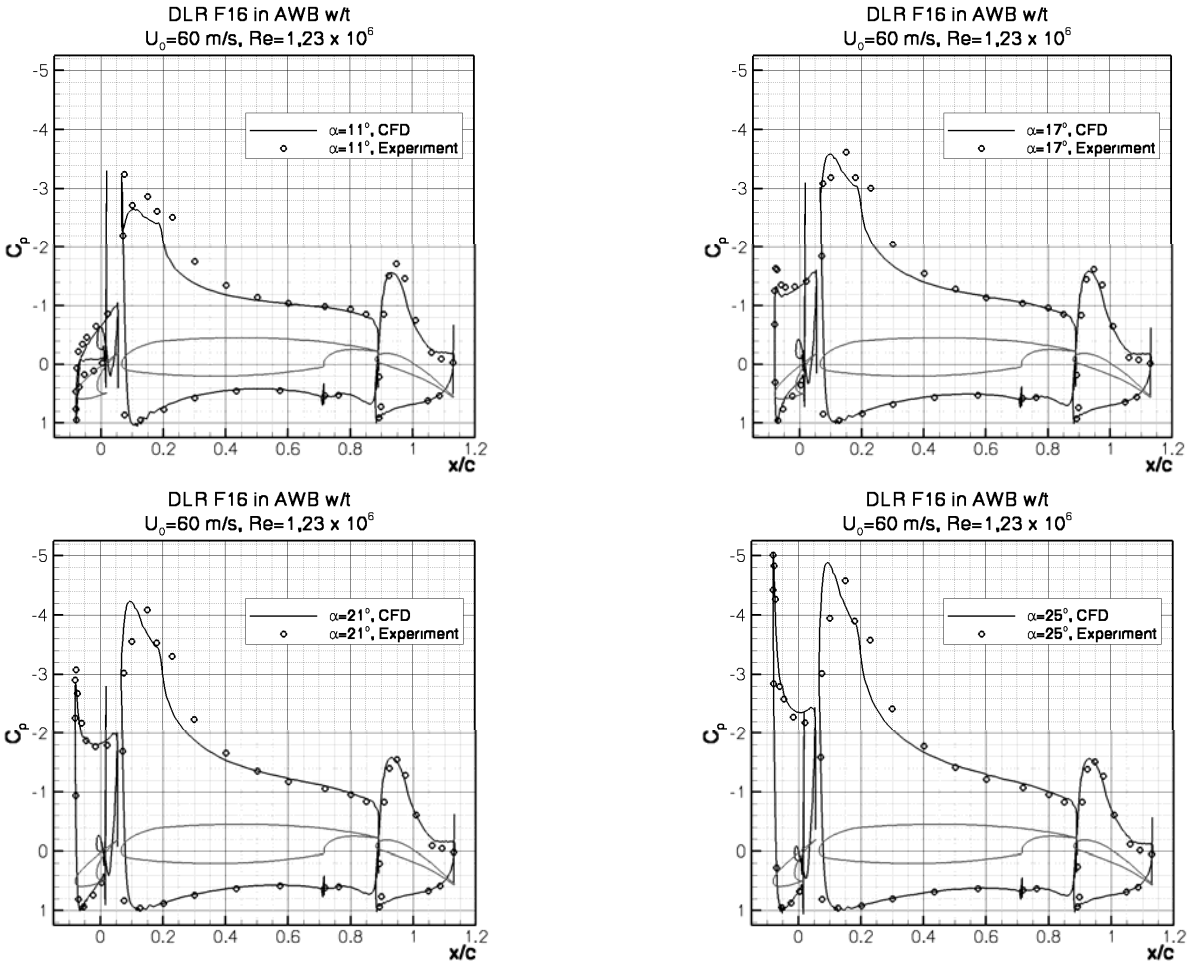

Figure 14 DLR F16 pressure distribution

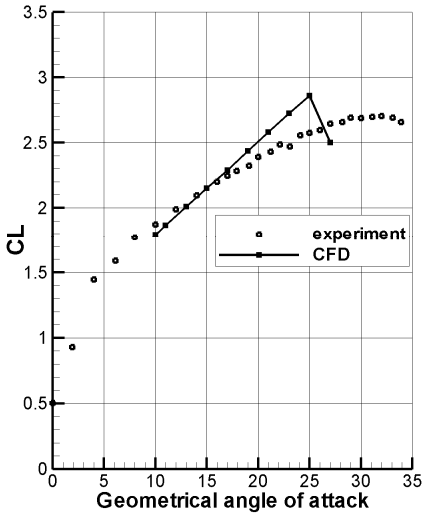

Figure 15 Lift curve for DLR F16

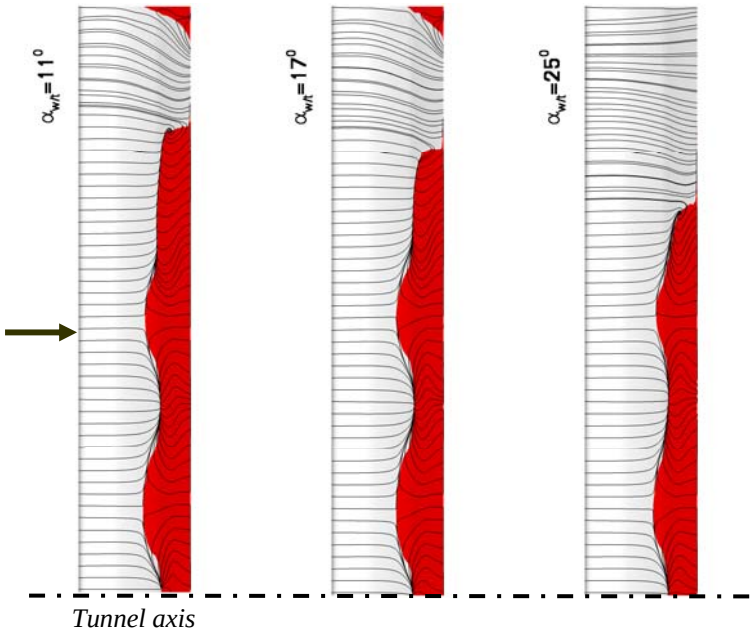

Figure 16 Flow separation on the flap of F16

Figure 17 Oil flow visualizations on the flap of the DLR F16 model

6 Conclusions

A process chain for the simulation of open wind tunnel test sections is presented in the paper based on investigations of the DLR project ForMEx II. ForMEx II is aimed at more accurate wind tunnel correction methods and improved extrapolation to free flight conditions by using CFD techniques. The results show that the numerical simulation is able to support the wind tunnel testing in open test sections. We may look now towards identifying the limits of the existing tunnel correction methods and further use these as a basis to improve today's wind tunnel testing techniques outlined here for the wind tunnels AWB and DNW-NWB.

For the simulations of the open flow test sections a new numerical approach for the tunnel speed control has been described. In order to verify the capability of the CFD technique to simulate the tunnel flows, detailed comparisons with the experiments have been presented for the jet velocity profiles, pressure distribution along the tunnel axis as well as for the boundary layer in the nozzle with empty tunnel configurations. A very good overall agreement was achieved, leading to confidence in simulating the open tunnel flows with experimental models.

The DLR 2D high-lift configuration F16 in the AWB tunnel was modelled including the supporting side plates. The impact of these walls is larger with an increased angle of attack. This trend and the separation region on the flap agree well with the experiments for moderate angles of attack. The slight differences in the separation regions achieved for high angles of attack and for the pressure distribution will be further investigated by taking into account the transition, and if requested a further mesh refinement study for the recirculation area. The results show the potential to simulate the flow for typical tunnel models in a justified time with the available modern CFD procedures. Not only that the numerical approach may serve for further improvement for the wind tunnel corrections, but also it may be used as a tool in advance of the wind tunnel testing.

Acknowledgments

The authors want to acknowledge the fruitful contribution from DNW-NWB's and AWB's colleagues involved in these experimental programmes.

7 Reference

[1] *The objectives of the DLR's ForMex Project.* G. Wichmann, European Wind tunnel Association (EWA), Initial Joint Workshop, ONERA, Toulouse, October 18-20, 2004.

[2] *A new approach in CFD supported Wind Tunnel Testing*. S. Melber-Wilkending, A. Heidebrecht and G. Wichmann, ICAS 2006.

[3] *www.**dnw**.aero*

[4] *An Integrated Design Approach for Low Noise Exposing High-Lift Devices*. J. Wild, M. Pott-Pollenske, B. Nagel. AIAA-2006-2843.

[5] MEGAFLOW - *A numerical Simulation Tool for Transport Aircraft Design*. N. Kroll, C.-C. Rossow, D. Schwamborn, K. Becker and G. Heller, 23rd ICAS Congress, Toronto, ICAS 2002, 1.5-10.5, 2002.

[6] *Two-Equations Eddy-Viscosity Turbulence Models for Engineering Applications.* F.R. Menter, AIAA Journal, 32(8):1598-1605, 1994.

[7] *Beeinflussung des statischen Druckes in der Offenen Messtrecke des Niedergeschwindigkeits-Windkanals Braunschweig (NWB)*. H. Otto, AG STAB, Jahresbuch 1993.